An Efficient Algorithm for SAR Evaluation from Anatomically Realistic Human Head Model Using DGTD with Hybrid Meshes

Lei Zhao [1,2], Geng Chen [1], and Wenhua Yu [1]

[1] Center for Computational Science and Engineering, School of Mathematics and Statistics
Jiangsu Normal University, Xuzhou, China
leizhao@jsnu.edu.cn, gengchn@163.com, yuwenhua@jsnu.edu.cn

[2] State Key Laboratory of Millimeter Waves, Southeast University, Nanjing, China

Abstract ─ In this paper, an efficient and fast algorithm is proposed to analyze the specific absorption rate (SAR) in the anatomically realistic human head model with voxel data format exposed a handset antenna. The algorithm is based on the discontinuous Galerkin time-domain (DGTD) method with conformal region division and hybrid meshes. The proposed algorithm is done by dividing the computational domain into a sub-region with head model and a sub-region with handset antenna. As the realistic head model is voxel data format, the voxel-based meshes are used to divide the sub-region with head model. The tetrahedral meshes are used to divide the antenna, and are suitable for antennas with curved features and thin objects. And the pyramid meshes are used to connect voxel-based mesh and tetrahedral mesh regions. The accuracy and efficiency of the proposed algorithm are verified by comparing numerical results with analytical solutions.

Index Terms ─ Anatomically realistic human head model, discontinuous Galerkin time-domain (DGTD), hybrid meshes, specific absorption rate (SAR).

I. INTRODUCTION

Electromagnetic energy absorption in human body exposed to electromagnetic radiation has brought about tremendous concerns for the possible consequences of electromagnetic radiation on human health in the past few decades. Many studies have been performed for calculating the RF specific absorption rate (SAR) in a human body exposed to the electromagnetic (EM) field [1-4]. The uncertainty of the calculated SAR distribution exists and is contributed by a number of factors including the implementation of numerical algorithm, the modeling of radiating source and the human head model. In the late 1970s, the human body was approximated as the composition of homogenous prolate spheroids, ellipsoids and cylinders. Then, the layered tissue models consisting of a few tissue types with different dielectric properties were used to approximate the human anatomy. Recently, a number of realistic partial or whole body human models have been created. Those voxel models can be constructed from cross-sectional images generated by computer tomography (CT) or magnetic resonance imaging (MRI), and the feature size and the number of tissues, and resolution of the model play an important role in the SAR calculation.

For voxel human body models, the finite difference time domain (FDTD) [5] is widely used to analyze the SAR in head model exposed to antennas. However, the FDTD method with Yee grid suffers from serious accuracy degradation for dealing with the curved objects or treating curved material interfaces [6]. A number of finite difference methods have been proposed in the past for the treatment of curved interfaces or complex objects [7-9]. Indeed, the so-called stair-casing approximation may lead to local zeroth-order and at most first-order accuracy, which may also produce locally non-convergent results. DGTD algorithm has most of the advantages of FDTD. Besides and contains the adaptability of the unstructured meshes and spatial super-convergence, which allows us to effectively handle many practical electromagnetic (EM) problems where the required precision is different over the entire domain, or when the solution lacks smoothness [10-13]. For SAR evaluation, Hassan uses DGTD method to calculate SAR of human head with tetrahedral mesh in their paper, the head model contains four kinds of tissues [14].

In this paper, the electromagnetic scattering problem from a high resolution 3D anatomically realistic head model was considered. The DGTD with hybrid meshes is proposed to analyze the SAR in the anatomically realistic head model exposed to a handset antenna. In the proposed algorithm, the computational domain is divided into two sub-regions. One sub-region includes head model and voxel-based grids are used for the simulation. Another sub-region includes the antenna and the tetrahedral meshes are used to describe the antenna with curved features and thin objects. And the pyramid meshes are used to connect voxel-based mesh

Submitted On: November 19, 2015
Accepted On: February 25, 2016

with tetrahedral mesh regions. We have verified the accuracy and efficiency of the algorithm by comparing the numerical results with analytical results. Numerical results show that the proposed method has a better performance than the conventional techniques.

II. THEORY AND METHOD

A. Governing equations and DGTD formulation

We consider the time-domain Maxwell equations in three space dimensions for heterogeneous linear isotropic media:

$$\varepsilon \frac{\partial \mathbf{E}}{\partial t} = \nabla \times \mathbf{H} - \sigma \mathbf{E} + \mathbf{J}, \tag{1}$$

$$\mu \frac{\partial \mathbf{H}}{\partial t} = -\nabla \times \mathbf{E}, \tag{2}$$

where $\mathbf{E}(\mathbf{x},t) = (E^x, E^y, E^z)$, $\mathbf{H}(\mathbf{x},t) = (H^x, H^y, H^z)$ are the electric and magnetic fields, ε, μ, σ denote dielectric permittivity, magnetic permeability and conductivity respectively, and **J** represents the current density. This system of equations is supplemented with appropriate boundary conditions. Two different boundary conditions are involved in the examples considered in this work: perfect electrical conductor (PEC) and non-reflecting boundary. On the PEC surface, the tangential component of the electric field vanishes and the condition $\mathbf{n}\times\mathbf{E}=0$ is applied, where **n** denotes the unit normal vector to the PEC surface. For problems posed on unbounded domains, the computational domain is truncated and a uniaxial perfectly matched layer (UPML) is imposed on the truncated boundary [13].

We first discretize the computational domain Ω into a set of elements τ_i and,

$$\Omega \approx \Omega_h = \bigcup_{i=1}^{N_h} \tau_i . \tag{3}$$

For each element τ_i, the local electric and magnetic fields $\mathbf{E}_i$ and $\mathbf{H}_i$ are expressed as linear combination of linearly independent vector Φ_{il} $(1 \le l \le 3d_i)$:

$$\mathbf{E}_i(\mathbf{x},t) = \sum_{l=1}^{3d_i} E_{il}(t)\Phi_{il}(\mathbf{x}), \tag{4}$$

$$\mathbf{H}_i(\mathbf{x},t) = \sum_{l=1}^{3d_i} H_{il}(t)\Phi_{il}(\mathbf{x}), \tag{5}$$

where d_i is the local number of degrees of freedom and associates to the interpolation degree of p_i, and E_{il}, H_{il} denote the nodal values of $\mathbf{E}_i$ and $\mathbf{H}_i$, respectively. The global solution of Maxwell's Eqs. (1)–(2) is given by:

$$\mathbf{E}(\mathbf{x},t) \approx \mathbf{E}_h(\mathbf{x},t) = \bigoplus_{i=1}^{N_h} \mathbf{E}_i(\mathbf{x},t), \tag{6}$$

$$\mathbf{H}(\mathbf{x},t) \approx \mathbf{H}_h(\mathbf{x},t) = \bigoplus_{i=1}^{N_h} \mathbf{H}_i(\mathbf{x},t). \tag{7}$$

To avoid any ambiguity, we introduce the following notations:

$$(\Phi_{il})_{1\le l\le 3d_i} = \left[\begin{pmatrix} \varphi_{i1} \\ 0 \\ 0 \end{pmatrix}, \begin{pmatrix} 0 \\ \varphi_{i1} \\ 0 \end{pmatrix}, \begin{pmatrix} 0 \\ 0 \\ \varphi_{i1} \end{pmatrix}, \cdots, \begin{pmatrix} \varphi_{id_i} \\ 0 \\ 0 \end{pmatrix}, \begin{pmatrix} 0 \\ \varphi_{id_i} \\ 0 \end{pmatrix}, \begin{pmatrix} 0 \\ 0 \\ \varphi_{id_i} \end{pmatrix} \right], \tag{8}$$

$$(E_{il})_{1\le l\le 3d_i} = \left(E^x_{i1}, E^y_{i1}, E^z_{i1}, \cdots, E^x_{id_i}, E^y_{id_i}, E^z_{id_i}\right), \tag{9}$$

and similarly for the sequence $(H_{il})_{1\le l\le 3d_i}$.

Multiplying Eqs. (1)-(2) by the test function Φ, we get:

$$\int_{\tau_i} \varepsilon \frac{\partial \mathbf{E}}{\partial t} \cdot \Phi d\mathbf{x} = \int_{\tau_i} \nabla \times \mathbf{H} \cdot \Phi d\mathbf{x} - \int_{\tau_i} \sigma \mathbf{E} \cdot \Phi d\mathbf{x}, \tag{10}$$

$$\int_{\tau_i} \mu \frac{\partial \mathbf{H}}{\partial t} \cdot \Phi d\mathbf{x} = \int_{\tau_i} -\nabla \times \mathbf{E} \cdot \Phi d\mathbf{x}. \tag{11}$$

Integrating by part Eqs. (10)-(11), we have:

$$\int_{\tau_i} \varepsilon \frac{\partial \mathbf{E}_h}{\partial t} \cdot \Phi d\mathbf{x} = \int_{\tau_i} \nabla \times \Phi \cdot \mathbf{H}_h d\mathbf{x} - \int_{\partial \tau_i} \Phi \cdot (\mathbf{H}_h \times \mathbf{n}) ds - \int_{\tau_i} \sigma \mathbf{E}_h \cdot \Phi d\mathbf{x}, \tag{12}$$

$$\int_{\tau_i} \mu \frac{\partial \mathbf{H}_h}{\partial t} \cdot \Phi d\mathbf{x} = -\int_{\tau_i} \nabla \times \Phi \cdot \mathbf{E}_h d\mathbf{x} + \int_{\partial \tau_i} \Phi \cdot (\mathbf{E}_h \times \mathbf{n}) ds, \tag{13}$$

where **n** is the unit outward normal vector of faces on τ_i. In the DGTD method $\mathbf{E}_i$ and $\mathbf{H}_i$ on element boundary can be discontinuous across the boundary. For two distinct elements τ_i and τ_k in Ω_h, then let $a_{ik} = \tau_i \bigcap \tau_k$ be the common interface of τ_i and τ_k. Here we use the central flux, which is defined as follows:

$$\mathbf{E}_h \mid a_{ik} = \frac{\mathbf{E}_i \mid a_{ik} + \mathbf{E}_k \mid a_{ik}}{2}, \mathbf{H}_h \mid a_{ik} = \frac{\mathbf{H}_i \mid a_{ik} + \mathbf{H}_k \mid a_{ik}}{2}. \tag{14}$$

Evaluating the volume integrals and surface integrals in Eqs. (12)-(13) with central flux and re-integrating by parts, we can obtain:

$$\int_{\tau_i} \varepsilon \frac{\partial \mathbf{E}_h}{\partial t} \cdot \Phi d\mathbf{x} = \frac{1}{2}\int_{\tau_i} \nabla \times \Phi \cdot \mathbf{H}_h + \int_{\tau_i} \nabla \times \mathbf{H} \cdot \Phi d\mathbf{x} - \int_{\partial \tau_i} \Phi \cdot (\mathbf{H}_h \times \mathbf{n}) ds - \int_{\tau_i} \sigma \mathbf{E}_h \cdot \Phi d\mathbf{x}, \tag{15}$$

$$\int_{\tau_i} \mu \frac{\partial \mathbf{H}_h}{\partial t} \cdot \Phi d\mathbf{x} = -\frac{1}{2}\int_{\tau_i} \nabla \times \Phi \cdot \mathbf{E}_h + \nabla \times \mathbf{E} \cdot \Phi d\mathbf{x} + \frac{1}{2}\sum_{k\in v_i} \int_{\partial a_{ik}} \Phi \cdot (\mathbf{E}_h \times \mathbf{n}) ds. \tag{16}$$

Replace $\mathbf{E}_h$, $\mathbf{H}_h$ and Φ in Eqs. (15)-(16) by $(E_{il})_{1\le l\le 3d_i}$, $(H_{il})_{1\le l\le 3d_i}$ and $(\Phi_{il})_{1\le l\le 3d_i}$, respectively, we can get an equivalent system:

$$M_i^{\varepsilon} \partial_t E_i = K_i H_i - \sum_{k\in v_i} S_{ik} H_k - D_i E_i, \tag{17}$$

$$M_i^{\mu} \partial_t H_i = -K_i E_i + \sum_{k\in v_i} S_{ik} E_k, \tag{18}$$

in which M_i^{ε} and M_i^{μ} are the symmetric positive definite mass matrices, K_i, S_{ik} and D_i are stiffness matrix, rectangular interface matrices and conduction matrix, respectively. They are defined as:

$$\left(M_i^{\varepsilon}\right)_{jl} = \int_{\tau_i} \Phi_{ij}^T \varepsilon_i \Phi_{il} d\mathbf{x} \qquad \left(1 \le j,l \le 3d_i\right), \quad (19)$$

$$\left(M_i^{\mu}\right)_{jl} = \int_{\tau_i} \Phi_{ij}^T \mu_i \Phi_{il} d\mathbf{x} \qquad \left(1 \le j,l \le 3d_i\right), \quad (20)$$

$$\left(K_i\right)_{jl} = \frac{1}{2}\int_{\tau_i} \Phi_{ij}^T \nabla \times \Phi_{il} + \Phi_{il}^T \cdot \nabla \times \Phi_{ij} d\mathbf{x} \left(1 \le j,l \le 3d_i\right), \quad (21)$$

$$\left(S_{ik}\right)_{jl} = \frac{1}{2}\int_{\tau_i} \Phi_{ij}^T \left(\Phi_{kl} \times \mathbf{n}_{ik}\right) ds \left(1 \le j \le 3d_i, 1 \le l \le 3d_k\right), \quad (22)$$

$$\left(D_i\right)_{jl} = \int_{\tau_i} \Phi_{ij}^T \sigma_i \Phi_{il} d\mathbf{x} \quad \left(1 \le j,l \le 3d_i\right). \quad (23)$$

The set of local system of ordinary differential equations for each τ_i can be formally transformed in a global system. We suppose that all electric and magnetic fields are gathered in a column vector $\mathbb{E}$ and $\mathbb{H}$ with size of $d = \sum_{i=1}^{N_h} d_i$. Then Eqs. (17)-(18) can be rewritten as:

$$\mathbb{M}_{\varepsilon} \frac{d\mathbb{E}}{dt} = \mathbb{K}\mathbb{H} - \mathbb{A}\mathbb{H} - \mathbb{B}\mathbb{H} - \mathbb{C}^E\mathbb{E} - \mathbb{D}\mathbb{E}, \quad (24)$$

$$\mathbb{M}_{\mu} \frac{d\mathbb{H}}{dt} = -\mathbb{K}\mathbb{E} + \mathbb{A}\mathbb{E} - \mathbb{B}\mathbb{E} + \mathbb{C}^H\mathbb{H}, \quad (25)$$

where $\mathbb{M}_{\varepsilon}$, $\mathbb{M}_{\mu}$ and $\mathbb{K}$ are $3d \times 3d$ block diagonal mass and stiffness matrices with diagonal blocks equal to M_i^{ε}, M_i^{μ} and K_i respectively. $\mathbb{A}$ is a block sparse matrix whose non-zero blocks are equal to S_{ik} when a_{ik} is an internal interface. $\mathbb{C}^E$ and $\mathbb{C}^H$ are the block diagonal matrices associated with boundary integral terms. $\mathbb{D}$ is a positive semi-definite block diagonal matrix with diagonal blocks equal to D_i.

The semi-discrete system Eqs. (24)-(25) is time integrated using a second order leap-frog scheme as:

$$\mathbb{M}_{\varepsilon}\left(\frac{\mathbb{E}^{n+1} - \mathbb{E}^n}{\Delta t/2}\right) = \mathbb{S}\mathbb{H}^{n+\frac{1}{2}} + \mathbb{C}^E\mathbb{E}^n - \frac{1}{2}\mathbb{D}\left(\mathbb{E}^{n+1} + \mathbb{E}^n\right), \quad (26)$$

$$\mathbb{M}_{\mu}\left(\frac{\mathbb{H}^{n+\frac{3}{2}} - \mathbb{H}^{n+\frac{1}{2}}}{\Delta t/2}\right) = -\mathbb{S}^T\mathbb{E}^{n+1} + \mathbb{C}^H\mathbb{E}^n, \quad (27)$$

where $\mathbb{S} = \mathbb{K} - \mathbb{A} - \mathbb{B}$ and $\Delta t = t_n - t_{n-1}$ denotes the time step size. This algorithm is conditionally stable with a critical time step size proportional to h^{-1}. And the time step is determined by the smallest grid element as:

$$\Delta t \le \frac{2}{\sqrt{\rho\left(\left(\left(\mathbb{M}_{\mu}^{-1}\right)^{\frac{1}{2}}\right)^T \mathbb{S}\left(\mathbb{M}_{\varepsilon}^{-1}\right)^{\frac{1}{2}}\right)}}. \quad (28)$$

B. Hybrid meshes and basis functions

For the SAR calculation from anatomically realistic human head model exposed handset antenna, as shown in Fig. 1, a hybrid mesh approach [15, 16] is adopted in which an unstructured tetrahedral or pyramid mesh is used to discretize the sub-region containing the handset model, a structured Cartesian mesh is used to discretize the remainder of the computation domain containing the voxel head model. In three dimensions, the nodal distribution proposed in [10] for the tetrahedron and in [16] for the pyramid is used. A tensor product of one-dimensional Gauss-Lobatto points is used for hexahedron. Figure 2 shows the reference tetrahedron, pyramid and hexahedron with a nodal distribution corresponding to polynomial order $p = 2$.

For tetrahedron meshes, the basis function on reference element is described as:

$$\varphi_{i,j,k} = P_i^{0,0}\left(\frac{2x}{1-y-z} - 1\right)\left(1-y-z\right)^i P_j^{2i+1,0}\left(\frac{2y}{1-z} - 1\right) \left(1-z\right)^j P_k^{2i+2j+2,0}\left(2z-1\right), \quad i+j+k \le r \quad (29)$$

For pyramid meshes, the basis function on reference element is:

$$\varphi_{i,j,k} = P_i^{0,0}\left(\frac{x}{1-z}\right) P_j^{0,0}\left(\frac{y}{1-z} - 1\right)\left(1-z\right)^{\max(i,j)} P_k^{2\max(i,j)+2,\,0}\left(2z-1\right), \quad 0 \le i,j \le r-k, k \le r \quad (30)$$

And the following basis function is used for hexahedron meshes:

$$\varphi_{i,j,k} = \psi_i\left(x\right)\psi_j\left(y\right)\psi_k\left(z\right), \quad (31)$$

where $\psi_i\left(x\right) = \frac{\prod_{i \ne j} x - \xi_j}{\prod_{i \ne j} \xi_i - \xi_j}$ is the Lagrange interpolation function.

With this approach, the benefits of using affine elements can be exploited, not only for tetrahedral but also for the hexahedral and pyramidal elements. Moreover, compared to tetrahedral meshes, the use of hexahedral meshes results in a significant reduction in the number of internal faces. It can be expected that hybrid meshes will lead to a reduction in the CPU time requirements, as the computational cost of integration over element faces is an important portion of the DGTD scheme.

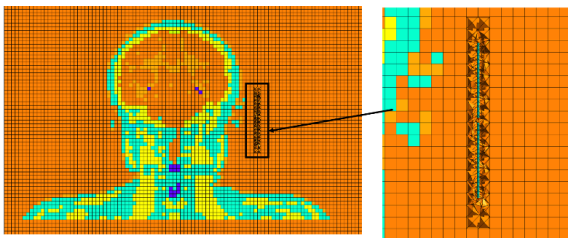

Fig. 1 Human head model exposed in dipole antenna.

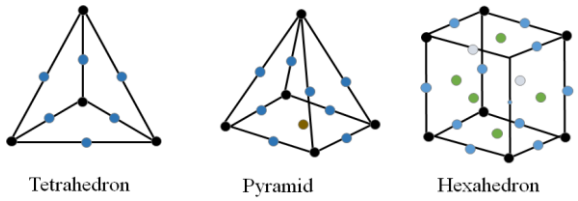

Fig. 2. Reference elements with showing the location of the nodes: (a) tetrahedron, (b) pyramid, and (c) hexahedron.

III. NUMERICAL RESULTS

To illustrate the accuracy and efficiency of the proposed DGTD with hybrid meshes, we first consider the EM propagation of a mode inside a perfect metallic cubic cavity. The cavity is a cube with a PEC boundary, the edge length of the cube is $1m$ with the center at $x = y = z = 0$. We evaluate the field at a test-point $x = y = z = -0.167m$. The propagative mode is given by following formulations:

$$\begin{aligned} E_x &= 0, \\ E_y &= 0, \\ E_z &= \sin(m\pi x)\sin(m\pi x)\cos(\omega t), \\ H_x &= \frac{1}{\omega\mu_0} n\pi \sin(m\pi x)\cos(m\pi x)\sin(\omega t), \\ H_y &= \frac{1}{\omega\mu_0} m\pi \cos(m\pi x)\sin(m\pi x)\sin(\omega t), \\ H_z &= 0. \end{aligned} \tag{32}$$

The comparison of numerical results of the internal electric fields obtained by using DGTD with hexahedron mesh, the FDTD method and analytical results $(m = n = 2)$ is illustrated in Fig. 3, where the mesh size for DGTD and FDTD is $\lambda/10$. From Fig. 3, we clearly observe a very good agreement between the DGTD method and analytical results, which is much better than the FDTD results. We have also computed the electric fields at the observation point $x = y = z = -0.167m$ using DGTD with tetrahedron meshes and hybrid meshes, and the FDTD method with mesh size $\lambda/30$, as demonstrated in Fig. 4. Good agreements can be obtained between the GDTD results and analytic results. Comparing with analytic results, the FDTD method with mesh size $\lambda/30$ is much better than the FDTD results with mesh size $\lambda/10$, as shown in Fig. 3 and Fig. 4. However, the FDTD method with $\lambda/30$ cannot still get a good agreement with the analytic results. The detailed computational parameters such as mesh size, degrees of freedom, time step and computational time are listed in Table 1. The benefit of using hexahedron elements can be clearly seen in Table 1 by comparing the computational cost. The reason for the benefit obtained is that tetrahedral meshes possess more elements and more internal faces than hexahedral meshes for a given number of degrees of freedom in DG framework. Meanwhile, the computation of numerical fluxes at internal faces represents an important part of the overall computational cost of the algorithm. For the EM problems from simple 3D geometries, the potential computational advantages of hexahedral elements can often be exploited. However, this is totally unfeasible for complex geometries. For this reason, it is a good choice to use hybrid meshes, employing tetrahedral elements near objects of complex geometrical shape, with affine hexahedral elements used to fill the remainder of the computational domain.

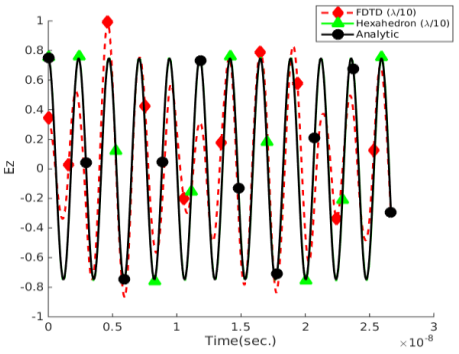

Fig. 3. Electric field distribution at point $x = y = z = -0.167m$.

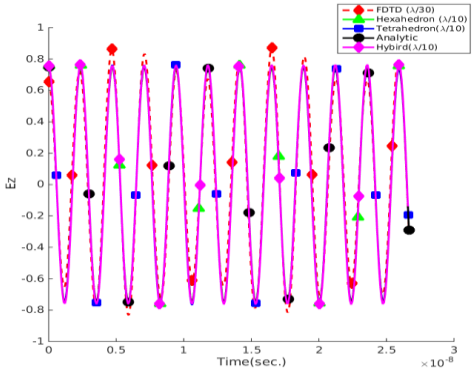

Fig. 4. Electric field distribution at point $x = y = z = -0.167m$.

Table 1: Mesh size, degrees of freedom, time step and computational time

Mesh Type	Mesh Size	Δt (s)	Dofs	CPU Time(s)
Tetrahedron	$\lambda/10$	0.021	18240	36.8
Hexahedron	$\lambda/10$	0.047	3375	1.2
Hybrid meshes	$\lambda/10$	0.028	5550	6.2
FDTD	$\lambda/10$	0.025	8000	0.2
FDTD	$\lambda/30$	0.01	216000	16.1

After verification of the accuracy and efficiency, we apply the proposed DGTD method with hybrid meshes to study the scattering problem from 3D anatomically realistic human head model exposed to a handset antenna, as shown in Fig. 5. The Chinese electromagnetic human model (CMODEL) used in the simulation setup is voxel format model, in which 15 different biological tissues can be identified, as shown in Fig. 6. The electromagnetic properties (ε_r and σ) of 15 different tissues in the model can be obtained from FCC directly [17], as listed in Table 2. The resolution of this model is 5 mm. The handset antenna is a half wave dipole working at 2.1 GHz, and the distance between head model and antenna is15 mm. To accurately describe the antenna, tetrahedral meshes are used for the sub-region containing the antenna. As the head model is voxel-based format, the hexahedral meshes are used to describe the sub-region containing the human head model. And two parts are connected by affine pyramid meshes.

As the dipole antenna has 15 degrees rotation, it is hard for the computational methods with cube grids to solve the problem. DGTD method with tetrahedral meshes is suitable to handle the EM problem from complex and thin objects. Figure 7 shows the return loss of the dipole antenna with 15 degree rotation, a good agreement can be obtained for different antenna postures.

To evaluate the performance of different elements employed for the numerical solution of the Maxwell's equations in three dimensions using a DGTD formulation, the tetrahedral and hybrid meshes are used to solve the EM problem of 3D anatomically realistic human head model exposed to an antenna, respectively. Table 3 shows the number of degrees of freedom and CPU time for solving the same problem with tetrahedral and hybrid meshes, where the mesh distributions are generated by using the same mesh size. It is observed that the reduction in number of degrees of freedom is translated into a corresponding reduction in computational cost. For an order of approximation p=2, hybrid elements provide the same accuracy as tetrahedral elements by reducing the CPU time by a factor of about 5, as shown in Table 3. Figure 8 shows the electric field distribution on the head surface, bone, brain and blood. The electric field distribution on slices of x=200 mm and y=170 mm is demonstrated in Fig. 7. The following definition of the point SAR value is used in this work [2]:

$$SAR = \frac{\sigma}{\rho}|\mathrm{E}|^2, \tag{33}$$

where σ is the electric conductivity, ρ the density of the tissue, and E the computed electric field intensity. The SAR distribution is shown in Fig. 9.

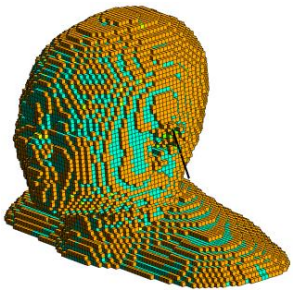

Fig. 5. CMODEL exposed to a dipole antenna working at 2.1 GHz.

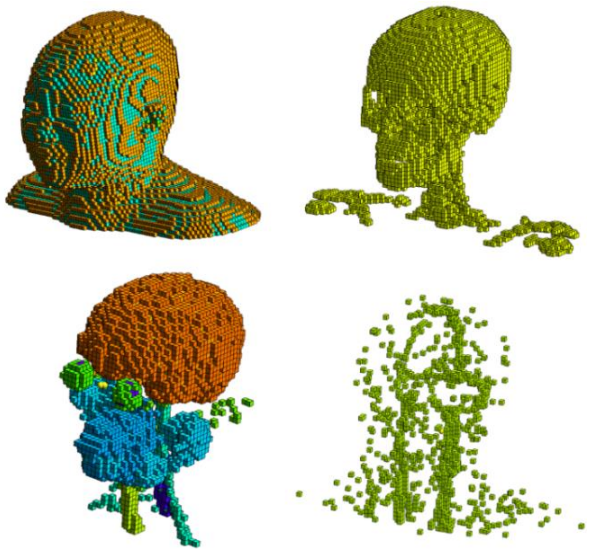

Fig. 6. CMODEL with 15 tissues.

Table 2: Dielectric properties of human head tissues at 2.1 GHz

Tissue	ε_r	σ
Skin	38.871857	1.184768
Fat	5.349368	0.078385
Muscle	55.335312	1.437796
Cartilage	40.215481	1.286782
Cerebro spinal fluid	68.638336	2.412575
Eye tissue	53.567787	1.601727
Vitreous humour	68.573364	2.032478
Lens nucleus	34.649647	0.787477
Grey matter	50.078876	1.391190
White matter	37.010921	0.914969
Spinal chord	32.530067	0.573612
Thyroid thymus	58.142151	1.500878
Tongue	53.567787	1.371193
Bone cancellous	19.343237	0.588224
Blood	59.372261	2.043690

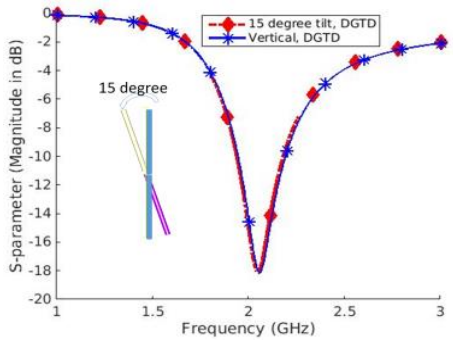

Fig. 7. Return loss for dipole antenna.

Table 3: Comparison of Dofs and computational cost with tetrahedron and hybrid meshes

Mesh Type	Δt (sec.)	Dofs	CPU Time(sec.)
Tetrahedron	0.53	24714168	60801
Hybrid Meshes	1.40	13355664	12819

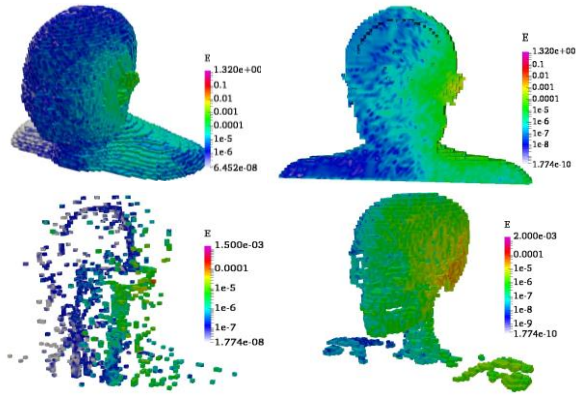

Fig. 8. Electric field distribution on tissues.

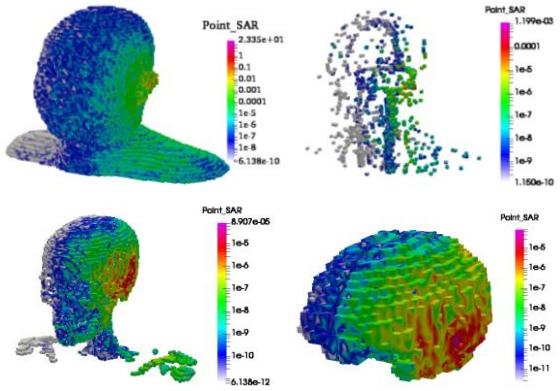

Fig. 9. Point SAR distribution.

IV. CONCLUSION

The efficiency of the DGTD method with hybrid mesh for the realistic human head SAR evaluation has been studied. Using an unstructured mesh around complex geometric objects, geometric flexibility is achieved. And computational efficiency is then improved by using a Cartesian mesh of affine hexahedra to fill the remainder of the domain.

ACKNOWLEDGMENT

This work was supported in part by the National Science Foundation of China under Grant No. 61372057, in part by the Open Project of State Key Laboratory of Millimeter Waves under Grant No. K201613.

REFERENCES

[1] A.-K. Lee, H.-D. Choi, and J.-I. Choi, "Study on SARs in head models with different shapes by age using SAM model for mobile phone exposure at 835 MHz," IEEE Trans. Electromagnetic Compatibility, vol. 49, pp. 302-312, 2007.

[2] A. Schiavoni, P. Bertotto, G. Richiardi, and P. Bielli, "SAR generated by commercial cellular phones-phone modeling, head modeling, and measurements," *IEEE Trans. Microwave Theory and Techniques*, vol. 48, pp. 2064-2071, 2000.

[3] L. Zhao and K.-L. Wu, "A Hybrid NFM/MoM full-wave analysis of layered proflate head model exposed to handset antenna," *Progress In Electromagnetics Research*, vol. 123, pp. 205-225, 2012.

[4] B. B. Beard, W. Kainz, T. Onishi, T. Iyama, S. Watanabe, O. Fujiwara, et al., "Comparisons of computed mobile phone induced SAR in the SAM phantom to that in anatomically correct models of the human head," *IEEE Trans. Electromagnetic Compatibility*, vol. 48, pp. 397-407, 2006.

[5] A. Taflove and S. Hagness, *Computational Electromagnetics: The Finite-Difference Time-Domain Method*, 3rd ed., Artech House, Norwood, MA, 2005.

[6] A. Ditkowski, K. Dridi, and J. S. Hesthaven, "Convergent Cartesian grid methods for Maxwell's equations in complex geometries," *Journal of Computational Physics*, vol. 170, pp. 39-80, 2001.

[7] T. Xiao and Q. H. Liu, "A staggered upwind embedded boundary (SUEB) method to eliminate the FDTD staircasing error," *IEEE Trans. Antennas and Propagation*, vol. 52, pp. 730-741, 2004.

[8] S. Chaillou, J. Wiart, and W. Tabbara, "A subgridding scheme based on mesh nesting for the FDTD method," *Microwave and Optical Technology Letters*, vol. 22, pp. 211-214, 1999.

[9] A. Yefet and P. G. Petropoulos, "A staggered fourth-order accurate explicit finite difference scheme for the time-domain Maxwell's equations," *Journal of Computational Physics*, vol. 168, pp. 286-315, 2001.

[10] J. S. Hesthaven and T. Warburton, "High–order nodal discontinuous Galerkin methods for the Maxwell eigenvalue problem," *Philosophical Transactions of the Royal Society of London A: Mathematical, Physical and Engineering Sciences*, vol. 362, pp. 493-524, 2004.
[11] G. Cohen, X. Ferrieres, and S. Pernet, "A spatial high-order hexahedral discontinuous Galerkin method to solve Maxwell's equations in time domain," *Journal of Computational Physics*, vol. 217, pp. 340-363, 2006.
[12] S. Pernet and X. Ferrières, "Hp a-priori error estimates for a non-dissipative spectral discontinuous Galerkin method to solve the Maxwell equations in the time domain," *Mathematics of Computation*, vol. 76, pp. 1801-1832, 2007.
[13] X. Ji, T. Lu, W. Cai, and P. Zhang, "Discontinuous galerkin time domain (DGTD) methods for the study of 2-D waveguide-coupled microring resonators," *Journal of Lightwave Technology*, vol. 23, pp. 3864, 2005.
[14] H. Fahs, A. Hadjem, S. Lanteri, J. Wiart, and M.-F. Wong, "Calculation of the SAR induced in head tissues using a high-order DGTD method and triangulated geometrical models," I*EEE Trans. Antennas and Propagation*, vol. 59, pp. 4669-4678, 2011.
[15] R. Sevilla, O. Hassan, and K. Morgan, "The use of hybrid meshes to improve the efficiency of a discontinuous Galerkin method for the solution of Maxwell's equations," *Computers and Structures*, vol. 137, pp. 2-13, 2014.
[16] M. Bergot, G. Cohen, and M. Duruflé, "Higher-order finite elements for hybrid meshes using new nodal pyramidal elements," *Journal of Scientific Computing*, vol. 42, pp. 345-381, 2010.
[17] https://transition.fcc.gov/oet/rfsafety/dielectric.html.

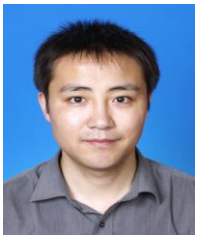

Lei Zhao joined the Jiangsu Normal University in September 2009. He is the Director of the Center for Computational Science and Engineering, and the Vice Dean of School of Mathematics and Statistics. He received the B.S. degree in Mathematics from Jiangsu Normal University, China, 1997, the M.S. degree in Computational Mathematics, and the Ph.D. degree in Electromagnetic Fields and Microwave Technology from Southeast University, China, in 2004 and 2007, respectively. From Aug. 2007 to Aug. 2009, he worked in Department of Electronics Engineering, The Chinese University of Hong Kong as a Research Associate. From Feb. 2011 to Apr. 2011, he worked in Department of Electronics and Computer Engineering, National University of Singapore as a research Fellow.

Zhao has published over 20 technical papers in PRE, APL, IEEE APM etc., international journals and conferences. His current research interests include computational electromagnetics, electromagnetic radiation to human's body, and numerical methods for partial differential equations.

Geng Chen received the B.S. degree and Master degree in Computational Mathematics from Jiangsu Normal University in 2012 and 2015, respectively. He is currently working at University of Illinois at Urbana-Champaign, USA, as a Research Assistant. His research interests include parallel-processing techniques, numerical methods, and software development.

Wenhua Yu joined the Jiangsu Normal University as a Distinguished Professor in May, 2014. He is the Director of the Jiangsu Key Laboratory for Education Big Data Science and Engineering. He worked at the Department of Electrical Engineering of the Pennsylvania State University and has been a Group Leader of the Electromagnetic Communication Lab between 1996 and 2013. He received his Ph.D. in Electrical Engineering from the Southwest Jiaotong University in 1994. He worked at the Beijing Institute of Technology as a Postdoctoral Research Associate from February 1995 to August 1996. He has published five books related to the FDTD method, parallel-processing techniques, software-development techniques, and simulation techniques, from 2003 to 2009. He has published over 150 technical papers and four book chapters. He founded the Computer and Communication Unlimited company, and serves as President and CEO. He is a Senior Member of the IEEE. His research interests include computational electromagnetic methods, software-development techniques, parallel-processing techniques, simulation and design of antennas, antenna arrays, and microwave circuits.